Monthly Notices
of the
ROYAL ASTRONOMICAL SOCIETY
MNRAS **443,** 3381–3387 (2014) doi:10.1093/mnras/stu1397

Dwarf galaxies in the Perseus Cluster: further evidence for a disc origin for dwarf ellipticals

Samantha J. Penny,[1,2]★ Duncan A. Forbes,[3] Kevin A. Pimbblet[1,2,4] and David J. E. Floyd[1,2]

[1]*School of Physics, Monash University, Clayton, VIC 3800, Australia*
[2]*Monash Centre for Astrophysics, Monash University, Clayton, VIC 3800, Australia*
[3]*Centre for Astrophysics and Supercomputing, Swinburne University of Technology, Hawthorn, VIC 3122, Australia*
[4] *Department of Physics and Mathematics, University of Hull, Cottingham Road, Kingston-upon-Hull HU6 7RX, UK*

Accepted 2014 July 8. Received 2014 July 7; in original form 2014 May 28

ABSTRACT

We present the results of a Keck-ESI (Echellette Spectrograph and Imager) spectroscopic study of six dwarf elliptical (dE) galaxies in the Perseus Cluster core, and confirm two dwarfs as cluster members for the first time. All six dEs follow the size–magnitude relation for dE/dSph galaxies. Central velocity dispersions are measured for three Perseus dwarfs in our sample, and all lie on the σ–luminosity relation for early-type, pressure-supported systems. We furthermore examine SA 0426-002, a unique dE in our sample with a bar-like morphology surrounded by low surface brightness wings/lobes ($\mu_B = 27$ mag arcsec^{-2}). Given its morphology, velocity dispersion ($\sigma_0 = 33.9 \pm 6.1$ km s^{-1}), velocity relative to the brightest cluster galaxy NGC 1275 (2711 km s^{-1}), size ($R_e = 2.1 \pm 0.10$ kpc), and Sérsic index ($n = 1.2 \pm 0.02$), we hypothesize the dwarf has morphologically transformed from a low-mass disc to dE via harassment. The low surface brightness lobes can be explained as a ring feature, with the bar formation triggered by tidal interactions via speed encounters with Perseus Cluster members. Alongside spiral structure found in dEs in Fornax and Virgo, SA 0426-002 provides crucial evidence that a fraction of bright dEs have a disc infall origin, and are not part of the primordial cluster population.

Key words: galaxies: clusters: general – galaxies: clusters: individual: Perseus Cluster – galaxies: dwarf – galaxies: evolution – galaxies: kinematics and dynamics – galaxies: structure.

1 INTRODUCTION

It is becoming increasingly clear that dwarf elliptical (dE) galaxies are not a simple, homogeneous galaxy population. Once thought to be the original building blocks in the hierarchical model of galaxy assembly that ceased their star formation early in the history of the Universe, dEs are instead found to exhibit a wide range of ages, metallicities, and morphologies inconsistent with a single primordial formation scenario (e.g. Penny & Conselice 2008; Lisker et al. 2009).

An alternative formation scenario is that a fraction of bright dEs are formed through the morphological transformation of low-mass, disc galaxies via processes such as harassment and ram pressure stripping as they infall into galaxy groups and clusters. Through harassment and interactions, the progenitor galaxy becomes morphologically transformed into a dE (Moore et al. 1996; Moore, Lake & Katz 1998; Mayer et al. 2001; Mastropietro et al. 2005; Villalobos et al. 2012). As the disc infalls into the cluster, it is stripped of its interstellar medium, and is dynamically heated by high-speed interactions with other galaxies and the gravitational potential of the cluster. To compensate, the galaxy loses stars, and over time the disc galaxy can morphologically transform into a dE. Evidence for this disc galaxy origin has been found in the form of embedded structures in cluster dEs such as bars and spiral arms (Jerjen, Kalnajs & Binggeli 2000; De Rijcke et al. 2003; Graham, Jerjen & Guzmán 2003; Lisker, Grebel & Binggeli 2006; Lisker & Fuchs 2009). Further evidence is provided in Kormendy & Bender (2012), who present two low mass discs in Virgo (NGC 4762 and NGC 4452) which show strong signatures for ongoing harassment in the form of warped outer isophotes.

During harassment, bar formation may be triggered via disc instabilities (Mastropietro et al. 2005; Aguerri & González-García 2009), and the galaxy will lose stars from its disc until only the bar remains. Examples of bar-like dwarfs that are likely the result of harassment are found in the Virgo Cluster, including VCC794, VCC1392, and VCC1567 (Graham et al. 2012). These galaxies are

★ E-mail: samantha.penny@monash.edu

sufficiently evolved that they show no evidence for ongoing mass-loss, with only their central bars remaining. Combined with observations of rotational, rather than pressure, supported dwarfs with rotation curves similar to those of star-forming galaxies (Toloba et al. 2011; Ryś, van de Ven & Falcón-Barroso 2014), evidence is mounting that a fraction of dEs originated as low-mass disc galaxies, and not as part of the primordial cluster population.

In this paper, we extend the study of dE kinematics to the Perseus Cluster, one of the richest and most relaxed galaxy clusters in the nearby Universe. As part of a wider study of dE kinematics across a range of environmental density (Penny et al., in preparation), we present Keck-ESI and *Hubble Space Telescope*-Advanced Camera for Surveys (*HST*-ACS) observations of a sample of nucleated dEs in the Perseus Cluster core ($D = 70$ Mpc) to examine their scaling relations. Here, we examine the kinematic properties of three dEs in the cluster core: two normal dEs (CGW 38 and CGW 39), and one unusual dE: SA 0426-002. We go on to establish morphological transformation via harassment as a possible formation scenario for SA 0426-002. First presented in Conselice, Gallagher & Wyse (2002), SA 0426-002 exhibits an unusual structure, with a strong bar-like morphology, no evidence for ongoing star formation, and low surface brightness 'wings' or 'lobes' surrounding the central bar. Conselice et al. (2002) noted that the dwarf is likely undergoing dynamical interaction, and merits further attention to uncover its nature and origin.

We describe our observations in Section 2, and present the results in Section 3, including the size–magnitude relation in Section 3.1. We discuss these results and the possibility of ongoing tidal evolution in Section 4, with our conclusion in Section 5.

2 OBSERVATIONS

2.1 Keck ESI spectrscopy

We observed bright dEs in the Perseus Cluster using the Echellette Spectrograph and Imager (ESI) instrument (Sheinis et al. 2002) on the Keck II telescope in echelle mode ($R \sim 8000$ for the 0.5 arcsec slit). Targets were selected from the catalogue of Conselice, Gallagher & Wyse (2003), with their cluster membership confirmed spectroscopically by Penny & Conselice (2008), else through dE-like morphology in *HST* imaging. Observations were taken on the nights 2012 November 5–7, with typical seeing 0.8 arcsec. We utilize the 0.5 arcsec slit, providing an instrument resolution $\sigma = 15.8\,\mathrm{km\,s^{-1}}$. The data provide complete wavelength coverage from 3900 to 10 000 Å over 10 orders. The data were reduced using standard calibration techniques with the automated MAKEE reduction package written by T. Barlow. Our spectroscopic observations are summarized in Table 1, with spectra in the region of the Hα feature for all six dwarfs shown in Fig. 1.

Table 1. Observing parameters.

Galaxy	S/N	Seeing (arcsec)	Exp. time (min)
SA 0426-002	7	0.8	80
CGW 20	5	0.7	120
CGW 38	10	0.6	90
CGW 39	10	0.7	60
CGW 40	5	0.5	150
CGW 45	5	0.6	80

Notes. S/N is the minimum signal-to-noise in the continuum at ∼8500 Å.

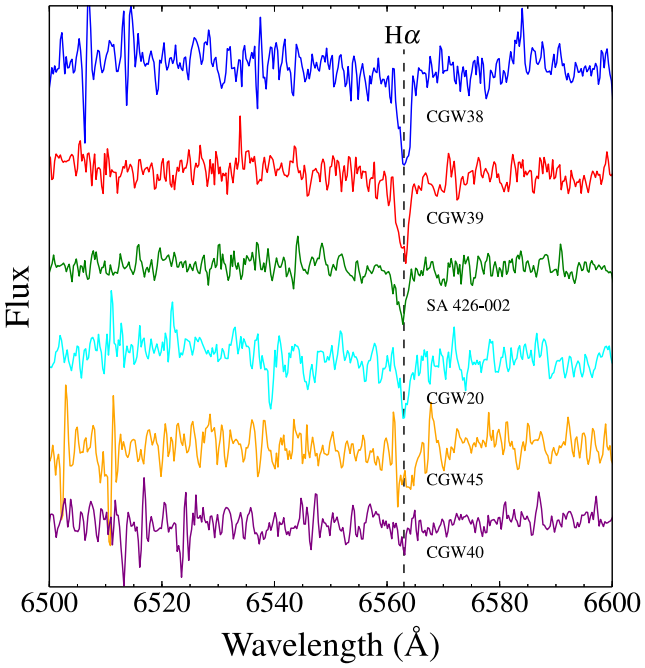

Figure 1. Keck-ESI spectra for the six Perseus dwarfs presented in this paper, trimmed to show the Hα features (ESI order 9). The spectra are corrected to rest wavelength using the velocities presented in Table 2. The spectra are sorted from top to bottom in order of decreasing S/N, and have not been smoothed.

Radial velocities for the target dEs were determined using the IRAF task FXCOR, utilizing the Fe/Mg (ESI order 12), Hα (ESI order 9), and CaT (ESI order 7) lines. We use standard stars taken under an identical observing setup as zero-redshift templates. We reconfirm cluster membership for four dwarfs with radial velocities measured by Penny & Conselice (2008), and confirm CGW 40 and SA 0426-002 as members of the Perseus Cluster for the first time.

2.2 *HST*-ACS imaging

To examine the morphology and scaling relations of SA 0426-002, we utilize high-resolution archival *HST*-ACS Wide Field Channel imaging (Fig. 2). The imaging was obtained in the *F625W* ($\sim R$) band, with a total exposure time of 2481 s, and a pixel scale 0.05 arcsec. The left-hand panel of Fig. 2 highlights features in the centre of the dwarf, including a bar-like morphology, and the model-subtracted image in the right-hand panel shows the low surface brightness wings/lobes exhibited by the dwarf. We utilize this high-resolution imaging to quantify the morphology of SA 0426-002 via an analysis of its light distribution.

3 RESULTS

3.1 The size–magnitude relation

To better understand the nature of SA 0426-002 compared to 'normal' dEs such as CGW 38 and CGW 39, we examine its scaling relations, including its location on the size–magnitude and σ–luminosity relations for early-type galaxies. First, we must determine the size of the dwarf. To do this, SA 0426-002 is modelled using GALFIT (Peng et al. 2002).

Given its proximity to the brightest cluster galaxy (BCG) NGC 1275, it was necessary to first remove the BCG's light to allow SA

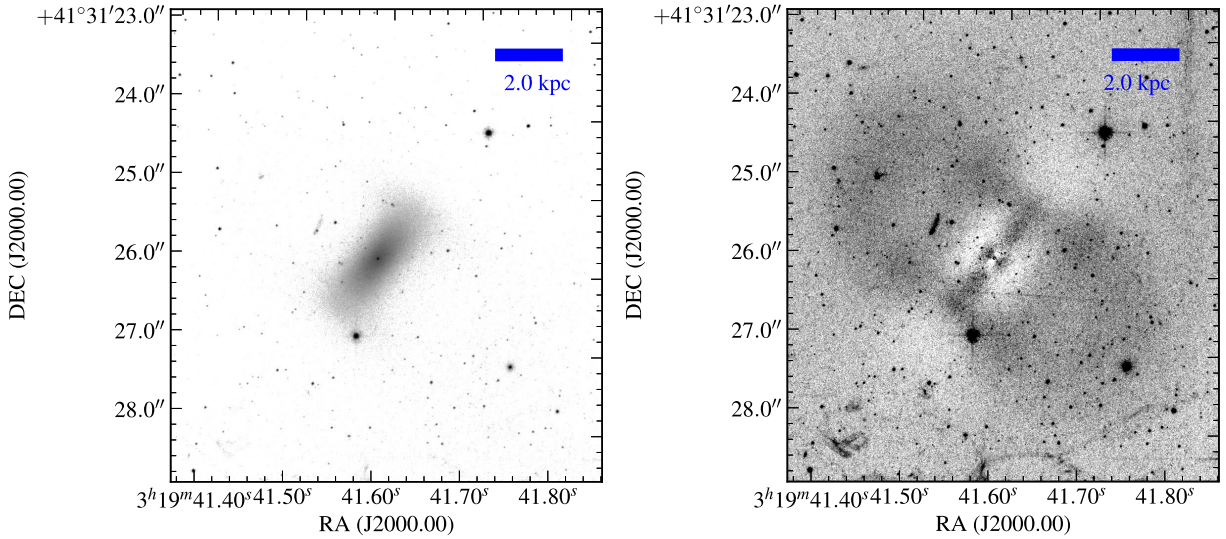

Figure 2. *HST*-ACS imaging of the Perseus Cluster dE SA 0426-002. The left-hand panel shows the dE with the background light from nearby NGC 1275 subtracted. The right-hand panel shows low surface brightness in the outer regions of the dE after the subtraction of the GALFIT model described in Section 3.1. A pair of low surface brightness lobes is clearly seen. These wings/lobes are likely a ring feature, which we hypothesize is the result of a tidal interaction with either a massive cluster galaxy or the cluster tidal potential.

0426-002 to be modelled accurately. We model NGC 1275 using a Sérsic model with a fixed Sérsic index of $n = 4$ and effective radius $R_e = 15$ kpc (Salomé et al. 2008), then subtract this model from the original image to remove the background gradient. SA 0426-002 was then modelled using a single profile Sérsic model convolved with the *HST*-ACS point spread function (PSF). The best-fitting model has Sérsic $n = 1.24 \pm 0.02$ and $R_e = 2.1 \pm 0.10$ kpc. The model of SA 0426-002 is elongated, with an axis ratio $b/a = 0.47 \pm 0.1$ ($\epsilon = 0.63$), and a boxy structure. The residuals of this model fit are shown in the right-hand panel of Fig. 2, revealing the wings/lobes that surround the dwarf.

We plot the newly calculated size of SA 0426-002 on the size–magnitude relation in Fig. 3, along with those of the Perseus dEs presented in this work, and a comparison sample of distance-confirmed early-type galaxies taken from the compilation of Brodie et al. (2011)[1] and references therein, with an update to this sample provided in Forbes et al. (2013) and references therein. The *V*-band magnitudes from Brodie et al. (2011) and Forbes et al. (2013) are converted to the *B* band using $(B - V) = 0.96$, a typical colour for an elliptical galaxy (Fukugita, Shimasaku & Ichikawa 1995). The sizes of the Perseus dwarfs in Fig. 3 are taken from Conselice et al. (2003) and de Rijcke et al. (2009), with the exception of SA 0426-002, which we calculate above.

The Brodie et al. (2011) sample contains a mix of compact ellipticals (cEs), dEs, and giant ellipticals (E), and the scaling relations of dEs and cE/E galaxies diverge at $M_B \approx -18$ (Kormendy 1985). To separate the galaxy populations, we highlight all galaxies classed as dE or dSph as purple circles. The sizes of the spectroscopically confirmed Perseus Cluster members agree with those of dEs in other studies, though we note SA 0426-002 is one of the largest dwarfs identified to date at its luminosity ($M_B = -16.3$). We will discuss a possible reason for this extended nature in Section 4.1.

[1] Available for download at sages.ucolick.org/spectral_database.html

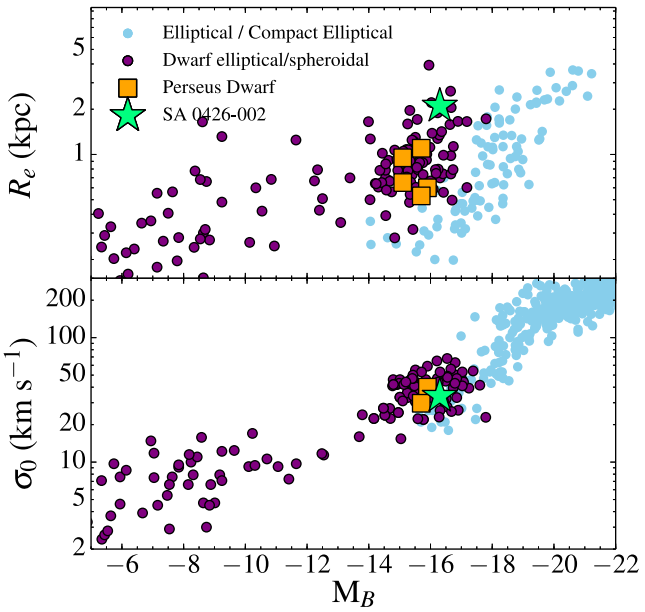

Figure 3. The size–magnitude relation (top panel) and σ–luminosity relation (bottom panel) for pressure supported systems with $R_e > 150$ pc. dE and dSph galaxies are plotted as purple dots to separate them from giant Es and cEs. We plot Perseus dEs with redshifts measured in this work as orange squares, and highlight the unusual dwarf SA 0426-002 as a green star. All the Perseus dEs lie on the size–magnitude and σ–luminosity relations for early-type galaxies.

3.2 Surface photometry

To examine the light distribution of SA 0426-002 in greater detail, the dwarf was modelled using the IRAF package ELLIPSE to fit isophotes to its light distribution. The position angle (PA), ellipticity (ϵ), and centre of the isophotes were allowed to vary during the fit. We show the results of this isophotal fit in Fig. 4, excluding

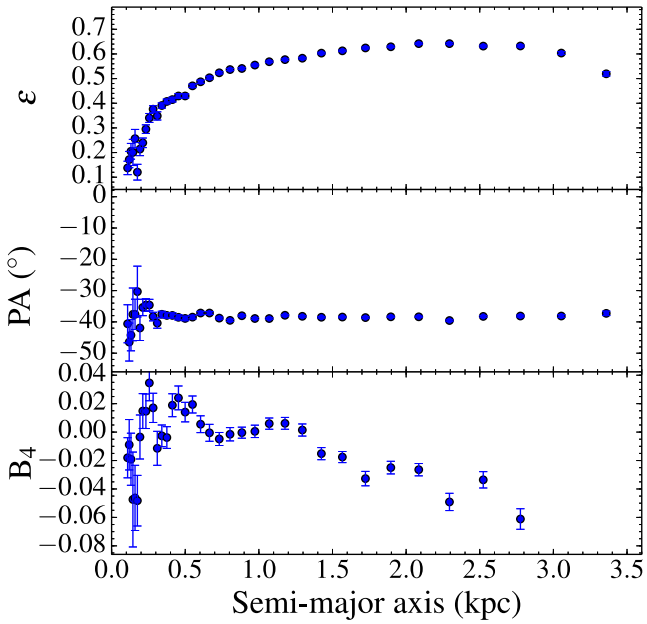

Figure 4. Light profile fits to SA 0426-002, showing the ellipticity (top panel), position angle (middle panel), and fourth harmonic amplitude $B4$ (bottom panel) as a function of semimajor axis. The dwarf becomes increasingly boxy ($B_4 < 0$) as the semimajor axis increases. Combined with elongated isophotes, this is consistent with its bar-like morphology. The position angle is constant with semimajor axis, and therefore the dwarf does not exhibit twists in its isophotes.

the inner 0.3 arcsec of the profile fit where the effect of the ACS PSF is strongest. The ellipticity (ϵ, top panel), position angle (PA, middle panel), and fourth harmonic amplitude $B4$ (bottom panel) are plotted as a function of semimajor axis to highlight the bar-like nature of the dwarf. The fourth harmonic amplitude $B4$ provides the deviation of the isophote from a perfect ellipse, with $B4 = 0$ for a perfect ellipse. Discy isophotes will have positive values of $B4$, while boxy isophotes will have negative values.

The position angle of the isophotal fit remains constant at PA $\approx -40^\circ$ out to the last plotted isophote at $R = 3.5$ kpc, with no evidence for warps/twists in the isophotes. In contrast, the dwarf's ellipticity changes from near circular in the centre of the galaxy, to elongated isophotes with $\epsilon = 0.63$ at $R = 2.5$ kpc. The discyness/boxiness of the dwarf furthermore changes dramatically over the structure of the bar feature, with the isophote's fourth harmonic amplitude $B4 \sim 0.02$ at $R = 0.5$ kpc (i.e. discy isophotes), compared to boxy isophotes with $B4 \sim -0.03$ at $R = 2.5$ kpc. These profiles highlight the dwarf's bar-like structure. These results are consistent with the surface photometry presented in Conselice et al. (2003).

3.3 Central velocity dispersions and dynamical masses

If a dE is formed via the morphological transformation and tidal stripping of a disc galaxy, we might expect it to have an unusually high velocity dispersion for its luminosity as σ_0 is expected to be relatively unchanged by the interaction (Bender, Burstein & Faber 1992), whereas its luminosity will be reduced. This will result in a high dynamical mass-to-light ratio for the dwarf. We therefore use our ESI spectroscopy to measure central velocity dispersions and dynamical masses for three dwarfs in our sample with a minimum signal-to-noise of 7 at ~8500 Å: SA 0426-002, CGW 38, and CGW 39.

To measure global internal velocity dispersions σ for the dEs, we use the Penalized Pixel Fitting (PPXF) routine (Cappellari & Emsellem 2004). We utilize five standard stars taken under an identical instrumental setup to the dwarf observations. The Fe, Mg, CaT, and Hα lines are used in determining the velocity dispersion for CGW 39, and the Hα line used for CGW 38 and SA 0426-002 due to the CaT feature blending with skylines. For SA 0426-002, we measure $\sigma = 32.4 \pm 5.5\,\mathrm{km\,s^{-1}}$. We measure $\sigma = 38.8 \pm 4.4\,\mathrm{km\,s^{-1}}$ for CGW 38, and $\sigma = 26.3 \pm 4.3\,\mathrm{km\,s^{-1}}$ for CGW 39. The errors are the formal errors provided by PPXF.

To compare our results to the literature, we convert these global values of σ to central values σ_0 at $R_e/8$ using equation 1 of Cappellari et al. (2006). These conversions are <10 per cent of the aperture velocity dispersion, and within the error bars of the uncorrected values of σ. For SA 0426-002, we find $\sigma_0 = 33.9 \pm 6.1\,\mathrm{km\,s^{-1}}$. CGW 38 has a central velocity dispersion $\sigma_0 = 40.0 \pm 5.5\,\mathrm{km\,s^{-1}}$, and for CGW 39, we determine a central velocity dispersion $\sigma_0 = 29.7 \pm 7.3\,\mathrm{km\,s^{-1}}$. We plot these central velocity dispersions in Fig. 3, along with a comparison sample taken from Penny et al. (2014). All three Perseus dEs lie on the σ–luminosity relation for early-type galaxies, and do not have unusual values of σ_0 for their magnitudes.

Using these central velocity dispersions, we calculate dynamical masses $M_{\rm dyn}$ for the three dEs using the expression

$$M_{\rm dyn} = C\sigma^2 R, \quad (1)$$

where R is the size of the galaxy, σ the object's velocity dispersion, and C is a correction for the object's light profile. For an exponential Sérsic brightness profile with $n = 1.0$ (typical for a dE galaxy), $C \approx 8$ (Bertin, Ciotti & Del Principe 2002) provides the total mass of the galaxy.

For SA 0426-002, this provides a dynamical mass $M_{\rm dyn} = (4.5 \pm 2.3) \times 10^9\ \mathrm{M_\odot}$. However, we note that given its strong bar-like structure, SA 0426-002 is likely rotating, and the conversion of the central velocity dispersion to a dynamical mass is therefore approximate. CGW 38 has $M_{\rm dyn} = (1.8 \pm 0.9) \times 10^9\ \mathrm{M_\odot}$, and CGW 39 has $M_{\rm dyn} = (8.9 \pm 0.5) \times 10^8\ \mathrm{M_\odot}$. These dynamical masses, along with the central velocity dispersions σ_0, are shown in Table 2.

3.4 Stellar masses and mass-to-light ratios

To investigate if any of the dwarfs have unusually high dynamical mass to stellar mass ratios (as might be expected for a tidally stripped object), we calculate stellar masses for all three dwarfs. This requires an estimation of both the ages and metallicities of the dwarfs' stellar populations, as the stellar mass-to-light ratio is dependent on both factors. Penny & Conselice (2008) estimate CGW 38 and CGW 39 to have old (>10 Gyr) stellar populations, with metallicities [Z/H] <−0.33 dex. To calculate stellar mass-to-light ratios, we utilize the SSP models of Bruzual & Charlot (2003), assuming a Salpeter initial mass function (IMF), a stellar age of 10 Gyr, and a metallicity [Fe/H] = −0.33 dex.

Based on these assumptions, CGW 38 and CGW 39 have B-band stellar mass-to-light ratios ~6. We note this ratio is an upper limit, as lower metallicity stellar populations will have lower stellar mass-to-light ratios. By converting their luminosities to stellar masses, we find $M_\star = (1.9 \pm 0.3) \times 10^9\ \mathrm{M_\odot}$ for CGW 38, and $M_\star = (1.7 \pm 0.5) \times 10^9\ \mathrm{M_\odot}$ for CGW 39. Errors are calculated based on the uncertainty in the ages and metallicities of the dwarfs' stellar populations. Within the error bars, these stellar masses are consistent with their dynamical masses.

Table 2. Properties of the Perseus dwarfs with spectroscopically confirmed cluster membership. The measured velocities and central velocity dispersions were determined from our Keck-ESI spectroscopy. The *B*-band magnitudes and sizes for the dwarfs are taken from Conselice et al. (2003), and De Rijcke et al. (2009), apart from SA 0426-002, which has its size determined in Section 3.1. Dynamical masses are calculated in Section 3.3.

Dwarf	α (J2000.0)	δ (J2000.0)	M_B (mag)	v (km s^{-1})	R_e (kpc)	σ_0 (km s^{-1})	M_{dyn} ($M_\odot$)	$M_\star$ ($M_\odot$)
SA 0426-002	03:19:40.00	+41:31:00.0	−16.3	7987 ± 15	2.1	33.9 ± 6.1	$(4.5 \pm 2.3) \times 10^9$	$(1.9 \pm 0.8) \times 10^9$
CGW 20	03:19:10.40	+41:29:37.0	−15.1	7325 ± 16	0.65	–	–	–
CGW 38	03:19:27.10	+41:27:16.1	−15.9	4205 ± 23	0.60	40.0 ± 5.5	$(1.8 \pm 0.9) \times 10^9$	$(1.9 \pm 0.3) \times 10^9$
CGW 39	03:19:31.40	+41:26:28.7	−15.7	6461 ± 24	0.53	29.7 ± 7.3	$(8.9 \pm 0.5) \times 10^8$	$(1.7 \pm 0.5) \times 10^9$
CGW 40	03:19:31.70	+41:31:21.3	−15.1	3763 ± 15	0.95	–	–	–
CGW 45	03:19:41.70	+41:29:17.0	−15.7	3156 ± 25	1.10	–	–	–

We repeat this stellar mass calculation for SA 0426-002. However, there is no estimation of the metallicity or age of this galaxy's stellar population. We therefore compare its colour to Bruzual & Charlot (2003) models to obtain the age of its stellar population, assuming an upper limit on its metallicity of [Fe/H] = −0.33 dex. SA 0426-002 has a colour $(B - R) = 1.3$ (Conselice et al. 2002). Comparing this colour to the Bruzual & Charlot (2003) stellar population synthesis models, the dwarf ceased star formation within the last 5 Gyr, and must be older than 1 Gyr.

Using the models of Bruzual & Charlot (2003), assuming a Salpeter IMF, an upper age limit 5 Gyr, and metallicity [Fe/H] ∼ −0.33, we estimate SA 0426-002 to have a maximum *B*-band stellar M/L ratio ∼3.6. This gives a stellar mass $(1.9 \pm 0.8) \times 10^9$ $M_\odot$. Its stellar mass is lower than its dynamical mass of $(4.5 \pm 1.6) \times 10^9$ $M_\odot$, giving a dynamical mass to stellar mass ratio of ∼2. This low mass-to-light ratio suggests the dwarf is unlikely to be dark-matter dominated in its inner regions, consistent with the results of Penny et al. (2009) for the mass-to-light ratios of bright dEs in Perseus. The stellar masses of all three dwarfs are listed in Table 2, along with errors based on uncertainties in the ages of the dwarfs.

4 DISCUSSION

All three Perseus dwarfs with measured kinematics have typical central velocity dispersions for their luminosities (Fig. 2), and lie on the size–magnitude relation for early-type galaxies, though SA 0426-002 is one of the most extended dwarfs at its luminosity. Given its unusual morphology (Fig. 2), we discuss this dwarf in greater detail.

SA 0426-002 is remarkably symmetric in appearance, with a bar-like morphology extending to $R \approx 2.8$ kpc (8 arcsec) from its nucleus. The central regions of the galaxy resemble an elongated dE with a boxy morphology. The galaxy has a nuclear star cluster, typical for bright dEs (Côté et al. 2006). However, the outer regions of this dE are highly unusual. Two symmetric, low surface brightness 'wings' can be seen either side of the main body of the galaxy (Fig. 2). Conselice et al. (2002) measure these wings to have $\mu_B = 27$ mag arcsec^{-2}. We discuss a possible origin for this unusual structure.

4.1 A tidally harassed galaxy?

SA 0426-002 is a unique dwarf galaxy, and the authors are unable to locate a dE with comparable morphology to SA 0426-002 in the literature. While bar-like dEs are known to exist in the Virgo Cluster (Graham et al. 2012), these dwarfs do not exhibit the low surface brightness lobes seen for SA 0426-002 in Sloan Digital Sky Survey (SDSS) imaging of comparable depth.

One possible explanation for this unusual morphology is that SA 0426-002 is being morphologically transformed from a low-mass disc or dwarf irregular to a dE via harassment. Due to multiple high-speed interactions with other cluster members, the infalling disc has been tidally perturbed, triggering bar formation. During this process, stars in the outer region of the disc are tidally stripped, forming arms/tidal features (e.g. Mastropietro et al. 2005), resulting in a high effective radius R_e for the galaxy's luminosity. Eventually, only the central bar will remain. We therefore hypothesize that SA 0426-002 has not yet had its disc completely stripped by high-speed interactions, and the low surface brightness wings are stars being tidally stripped from the galaxy.

Simulations of bar formation in tidally transforming discs have focused heavily on the Milky Way satellite system (e.g. Kazantzidis et al. 2011; Łokas et al. 2014). While NGC 1275 is more massive than the Milky Way, the tidal transformation of low-mass discs by its gravitational potential will progress in a similar, though more rapid, fashion, with bars forming on time-scales ∼1 Gyr (Mastropietro et al. 2005; Aguerri & González-García 2009). The simulations of Mayer et al. (2001) show that a rotationally supported, discy dIrr infalling into a MW-sized halo will form a bar with ring-like structures comparable to the morphology of SA 0426-002. Bar formation is rapid, occurring after the first pericentric approach (Łokas et al. 2014). The morphology of the dwarf is also remarkably similar to the simulations of Mastropietro et al. (2005), Aguerri & González-García (2009), and Villalobos et al. (2012), particularly for face-on views of simulated tidally interacting dwarfs. SA 0426-002 is likely a rare example of a dwarf mid-way through the morphological transformation from a disc to dE, and we are viewing this transformation face-on.

Aguerri & González-García (2009) present simulations of low-mass disc galaxies with varying bulge/disc ratios undergoing harassment in the cluster environment. The morphology of SA 0426-002 is remarkably similar to their simulated dwarfs whose progenitors have small bulge components and prograde rotation. In their simulations, Aguerri & González-García (2009) show that the scalelength of their discs will be reduced by 40–50 per cent after several tidal interactions, and the remnants will lie on the Fundamental Plane for dEs. The size–luminosity relation for dEs is consistent with that of a population of truncated disc galaxies (Boselli et al. 2008), further strengthening the argument that at least a fraction of dEs are tidally stripped disc galaxies. However, SA 0426-002 is extended for its luminosity on the size–magnitude relation presented in Fig. 3, and appears not to fit this scenario.

The fact that SA 0426-002 appears extended on the size–magnitude relation can be explained as we are likely seeing the dwarf early in its transformation from a disc to dE via harassment. The intracluster medium will rapidly ram-pressure strip a dwarf of its gas, and the dwarf will move to a fainter location on the size–magnitude relation, but it will have an extended size for its luminosity. SA 0426-002's colour $(B - R) = 1.3$ (Conselice et al. 2002) places it on the red sequence for dEs presented in Penny & Conselice (2008), and its Keck-ESI spectrum does not exhibit any emission lines consistent with ongoing star formation (e.g. Hα). This lack of star formation and red colour shows the dwarf has already been stripped of gas by the cluster environment. However, further tidal interactions are required to strip its mass, and hence decrease its effective radius. The ring feature in Fig. 2 can be easily destroyed by gravitational heating due to further tidal interactions in the cluster environment (Mastropietro et al. 2005), which will reduce the dwarf's effective radius.

Given its projected separation of 35 kpc from the BCG NGC 1275, could SA 0426-002 and the BCG be interacting? NGC 1275 is located at $v = 5276\,\mathrm{km\,s^{-1}}$ (Petrosian et al. 2007), with SA 0426-002 at $7987\,\mathrm{km\,s^{-1}}$. With a velocity separation of $2711\,\mathrm{km\,s^{-1}}$, the two galaxies are either undergoing a high-speed interaction, else SA 0426-002 is infalling into the cluster and interacting with the cluster tidal potential. Lisker et al. (2009) show that dwarfs with flattened morphologies (similar to SA 0426-002) in the Virgo Cluster typically have fast line-of-sight velocities, whereas spherical dEs are typically slow. In this scenario, this difference in morphology and velocity distributions for round versus flattened dwarfs is taken as evidence for an infall population with eccentric orbits. Flattened dwarfs represent the recent cluster infall population, whereas round dwarfs are the 'first' generation of cluster dEs which may have formed inside the primordial cluster itself.

4.2 A ring galaxy?

We consider the likelihood that SA 0436-002 is a ring galaxy. Examples of galaxies in the nearby Universe with comparable morphology to SA 0426-002 are ESO 325-28, ESO 509-98, and NGC 2665. However, these ring galaxies are massive, star-forming systems brighter than $M_B = -19.5$. Furthermore, SA 0436-002 lacks the spiral arms seen in these ring galaxies.

Given its strong bar-like morphology, a bar resonance has likely been set up in the galaxy at the outer Linblad resonance, resulting in the low surface brightness lobes either side of the central bar. The dwarf exhibits the characteristic 'dimpled' outer ring morphology, similar to the more inclined galaxy ESO 287-56 (Buta 1995). Gravitational torques from the bar can depopulate material at the corotation radius while building it up at the outer Lindblad radius. Thus, both a bar and gas in a disc are required to form the lobes or wings seen in SA 0426-002. We therefore hypothesize that the progenitor of SA 0426-002 was a dwarf disc galaxy, as gas is required to form the stars which make up the lobe features.

This ring galaxy morphology does not exclude ongoing tidal interactions; indeed, such interactions can trigger bar formation in an infalling disc galaxy. Mastropietro et al. (2005) show that infalling discs will undergo major structural transformation, including strong bar formation and spiral patterns. These spiral features will be stripped away, with remaining material forming a ring structure around the bar. Several galaxies in their simulations exhibit bar and ring features, and thus SA 0426-002 has characteristics of a ring galaxy formed via tidal harassment. Further tidal interactions within Perseus will likely remove the remaining ring structure, until only the bar of the galaxy remains, and such dwarfs are not uncommon in clusters (e.g. Graham et al. 2012).

5 CONCLUSIONS

Using the Keck-ESI spectrograph, we confirm two dEs as members of the Perseus Cluster (CGW 40 and SA 0426-002), and reconfirm cluster membership for four other dwarfs. The dwarfs lie on the size–magnitude relation for dEs, but SA 0426-002 has a large size for its magnitude, as it has ceased star formation but not yet been completely tidally stripped. We furthermore calculate central velocity dispersions and dynamical masses for three dwarfs in our sample: CGW 38, CGW 39, and SA 0426-002, and all three dwarfs follow the σ–luminosity relation for early-type stellar systems.

We examine the unusual dwarf SA 0426-002 in detail. SA 0426-002 exhibits a bar-like morphology with $R_e = 2.1 \pm 0.1$ kpc and Sérsic $n = 1.24 \pm 0.02$. Based on its bar-like morphology, ring structure, and its location in the Perseus Cluster, we hypothesize that SA 0426-002 is near its orbit pericentre, and is currently undergoing morphological transformation from a disc galaxy into a dE. The wing-like structure is the result of stellar mass loss due to tidal heating by repeated interactions with other cluster galaxies, else tidal interactions with the BCG NGC 1275.

Combined with embedded substructure identified in deep imaging of nearby dEs in Virgo (e.g. Lisker & Fuchs 2009) and Fornax (e.g. De Rijcke et al. 2003), it is becoming increasingly apparent that a fraction of dEs are not part of the primordial cluster population. Instead, these objects are formed at later times via the transformation of infalling disc galaxies.

ACKNOWLEDGEMENTS

SJP and KAP acknowledge the support of an Australian Research Council (ARC) Super Science Fellowship grant FS110200047. DAF thanks the ARC for support via DP130100388. We thank Michael J. I. Brown and Alister Graham for useful discussions. We also thank the referee for their thorough review which has improved the paper. The data presented herein were obtained at the W. M. Keck Observatory, which is operated as a scientific partnership among the California Institute of Technology, the University of California and the National Aeronautics and Space Administration. The Observatory was made possible by the generous financial support of the W. M. Keck Foundation. The authors wish to recognize and acknowledge the very significant cultural role and reverence that the summit of Mauna Kea has always had within the indigenous Hawaiian community, and we are most fortunate to have the opportunity to conduct observations from this mountain.

REFERENCES

Aguerri J. A. L., González-García A. C., 2009, A&A, 494, 891
Bender R., Burstein D., Faber S. M., 1992, ApJ, 399, 462
Bertin G., Ciotti L., Del Principe M., 2002, A&A, 386, 149
Boselli A., Boissier S., Cortese L., Gavazzi G., 2008, A&A, 489, 1015
Brodie J. P., Romanowsky A. J., Strader J., Forbes D. A., 2011, AJ, 142, 199
Bruzual G., Charlot S., 2003, MNRAS, 344, 1000
Buta R., 1995, ApJS, 96, 39
Cappellari M., Emsellem E., 2004, PASP, 116, 138
Cappellari M. et al., 2006, MNRAS, 366, 1126
Conselice C. J., Gallagher J. S., III, Wyse R. F. G., 2002, AJ, 123, 2246
Conselice C. J., Gallagher J. S., III, Wyse R. F. G., 2003, AJ, 125, 66
Côté P. et al., 2006, ApJS, 165, 57

De Rijcke S., Dejonghe H., Zeilinger W. W., Hau G. K. T., 2003, A&A, 400, 119
de Rijcke S., Penny S. J., Conselice C. J., Valcke S., Held E. V., 2009, MNRAS, 393, 798
Forbes D. A., Pota V., Usher C., Strader J., Romanowsky A. J., Brodie J. P., Arnold J. A., Spitler L. R., 2013, MNRAS, 435, L6
Fukugita M., Shimasaku K., Ichikawa T., 1995, PASP, 107, 945
Graham A. W., Jerjen H., Guzmán R., 2003, AJ, 126, 1787
Graham A. W., Spitler L. R., Forbes D. A., Lisker T., Moore B., Janz J., 2012, ApJ, 750, 121
Jerjen H., Kalnajs A., Binggeli B., 2000, A&A, 358, 845
Kazantzidis S., Łokas E. L., Callegari S., Mayer L., Moustakas L. A., 2011, ApJ, 726, 98
Kormendy J., 1985, ApJ, 295, 73
Kormendy J., Bender R., 2012, ApJS, 198, 2
Lisker T., Fuchs B., 2009, A&A, 501, 429
Lisker T., Grebel E. K., Binggeli B., 2006, AJ, 132, 497
Lisker T. et al., 2009, ApJ, 706, L124
Łokas E. L., Athanassoula E., Debattista V. P., Valluri M., del Pino A., Semczuk M., Gajda G., Kowalczyk K., 2014, preprint (arXiv:1404.1211)
Mastropietro C., Moore B., Mayer L., Debattista V. P., Piffaretti R., Stadel J., 2005, MNRAS, 364, 607
Mayer L., Governato F., Colpi M., Moore B., Quinn T., Wadsley J., Stadel J., Lake G., 2001, ApJ, 559, 754
Moore B., Katz N., Lake G., Dressler A., Oemler A., 1996, Nature, 379, 613
Moore B., Lake G., Katz N., 1998, ApJ, 495, 139
Peng C. Y., Ho L. C., Impey C. D., Rix H.-W., 2002, AJ, 124, 266
Penny S. J., Conselice C. J., 2008, MNRAS, 383, 247
Penny S. J., Conselice C. J., de Rijcke S., Held E. V., 2009, MNRAS, 393, 1054
Penny S. J., Forbes D. A., Strader J., Usher C., Brodie J. P., Romanowsky A. J., 2014, MNRAS, 439, 3808
Petrosian A., McLean B., Allen R. J., MacKenty J. W., 2007, ApJS, 170, 33
Ryś A., van de Ven G., Falcón-Barroso J., 2014, MNRAS, 439, 284
Salomé P., Revaz Y., Combes F., Pety J., Downes D., Edge A. C., Fabian A. C., 2008, A&A, 483, 793
Sheinis A. I., Bolte M., Epps H. W., Kibrick R. I., Miller J. S., Radovan M. V., Bigelow B. C., Sutin B. M., 2002, PASP, 114, 851
Toloba E., Boselli A., Cenarro A. J., Peletier R. F., Gorgas J., Gil de Paz A., Muñoz-Mateos J. C., 2011, A&A, 526, A114
Villalobos Á., De Lucia G., Borgani S., Murante G., 2012, MNRAS, 424, 2401

This paper has been typeset from a TEX/LATEX file prepared by the author.